Journal of Materials Science & Technology 70 (2021) 105–112

Contents lists available at ScienceDirect

Journal of Materials Science & Technology

journal homepage: www.jmst.org

Research Article

Atomic-scale roles of Zn element in age-hardened AlMgSiZn alloys

N.N. Jiao[a,1], Y.X. Lai[a,*,1], S.L. Chen[b], P. Gao[b], J.H. Chen[a,*]

[a] Center for High-Resolution Electron Microscopy, College of Materials Science & Engineering, Hunan University, Changsha, 410082, China
[b] Electron Microscopy Laboratory and International Center for Quantum Materials, School of Physics, Peking University, Beijing, 100871, China

ARTICLE INFO

Article history:
Received 22 April 2020
Received in revised form 7 June 2020
Accepted 7 July 2020
Available online 14 September 2020

Keywords:
Al-Mg-Si alloy
Zn addition
Precipitate
Electron microscopy

ABSTRACT

Adding alloying elements to improve the performances or the manufacturing processes of Al-Mg-Si alloys has long been a serious issue in developing advanced automotive aluminum materials. The Zn element, among those promising ones, has demonstrated positive alloying effects on Al-Mg-Si alloys. However, the atomic-scale roles of Zn in an age-hardened Al-Mg-Si-Zn alloy have not been adequately understood. Using atomic-resolution electron microscopy, here we report the precise locations of Zn elements in all hardening precipitates involved and their alloying mechanism at the atomic scale when alloying the alloy. Our results show that Zn atoms enter all the major hardening phases to occupy specific featured atomic sites of the original elements, e.g. the Si1 and Mg2 sites in the β'-2 phase, and modify their crystal structures, interfacial structures and morphologies in characteristic manners. It is revealed that for the β'-phase, Zn atoms occupy unique atomic sites, whereas for other phases, they demonstrate similar behaviors as other additive alloying elements such as Ag and Cu do.

1. Introduction

The heat-treatable Al-Mg-Si alloys are widely used in many industrial applications since they have advantageous properties: high strength-to-weight ratio, good formability and corrosion resistance [1,2]. The alloy's properties directly depend on nano-sized metastable precipitates formed with different crystal structures, sizes, number densities and volume fractions in the Al-matrix [3–5]. Therefore, considerable effort has gone into understanding the precipitation sequence as well as the precipitate crystal structures in the alloys. The precipitation sequence of Al-Mg-Si alloys is commonly described as [6,7]: supersaturated solid solution (SSSS)→ atomic clusters → GP zones → β" → β' (/B'/U1/U2) → β. The needle-like monoclinic β"-precipitates and their early-precursors, mostly formed in peak-aged conditions, are considered as the most effective hardening precipitates in Al-Mg-Si alloys [8–10]. The needle-like hexagonal β'-phase usually forms upon over-aging and sometimes is accompanied by precipitation of the B', U1 and U2 phases [11–15]. The β'-phase actually has two possible structures which may coexist in the same alloy [16], one is that with space group $P6_3/m$ and composition Mg_9Si_5 [11], and the other is called β'-2 structure with space group P-62 m and composition Mg_6Si_3 [16]. According to the above precipitation sequence, conventionally GP zone and β" are known as the early-stage hardening precipitate phases, whereas β' and B'/U1/U2 are considered as the late-stage hardening precipitate phases.

However, our recent studies have demonstrated that the phases formed in some Al-Mg-Si alloys are closely related to the composition of the alloy and the thermo-mechanical processes applied [17–19]. For example, β' forms directly without the formation of β̈during artificial aging at 180 °C in a lean alloy with solute content (Mg + Si) < 1 wt.% [17]. Moreover, when Cu is added into the alloy, another well-known hardening phase, called Q' (with space group $P6_3/m$ and composition $Al_3Cu_2Mg_9Si_7$) [20], may also appear in addition to the above mentioned phases.

Improving the performances or the manufacturing processes of Al-Mg-Si alloys by adding alloying elements has long been serious issues in developing advanced automotive aluminum materials. Among the alloying elements, Zn has been demonstrated to have a positive effect on the age-hardening response of Al-Mg-Si alloys and therefore has received much attention in recent years [21–23]. Although some studies reported that Zn addition to Al-Mg-Si alloys caused the formation of extra precipitates in the Al-*Zn*-Mg alloy system [23,24], most of recent investigations have shown that Zn atoms only influence formation of the precipitates previously known in the Al-Mg-Si(-Cu) alloy system [21,25,26]. The Zn addition leads to a finer and denser distribution of needle-shaped

* Corresponding authors.
E-mail addresses: lyxzhc123@hnu.edu.cn (Y.X. Lai), jhchen123@hnu.edu.cn (J.H. Chen).
[1] These authors equally contribute in this work.

https://doi.org/10.1016/j.jmst.2020.09.009
1005-0302/

precipitates, resulting in improved peak hardness [26]. In an effort to ascertain the role of Zn in the precipitate structures, researchers have employed high-angle annular dark-field scanning transmission electron microscopy (HAADF-STEM) and demonstrated that Zn can induce the formation of composite precipitates containing βänd other known phases in the Al-Mg-Si(-Cu) system [22]. HAADF-STEM imaging in association with first-principles calculations has indicated that Zn occupies the so-called Si3 sites in the β=phase structure with a partial occupation [27]. Nevertheless, the impact of Zn on the β'-type phases has not been clarified, which is a noteworthy issue since under circumstances these phases can be the main hardening phases of Al-Mg-Si alloys [17–19]. In fact, in the studies of the alloying effect of Ag addition to the Al-Mg-Si alloys, it has been reported that Ag atoms can modify the β'-2 structure in different manners [28,29].

In the present work, atomic-resolution HAADF-STEM characterization and first-principles calculations were employed to investigate the Zn alloying effect on the Al-Mg-Si alloy, with focusing on how Zn atoms would modify the microstructures of all hardening phases, especially on the β'-phase and its associated composite precipitates. Our study shows that for the β'-phase, Zn atoms occupy unique atomic sites, whereas for other phases, they demonstrate similar behaviors as other additive alloying elements such as Ag and Cu do.

2. Experimental and computational procedures

Two alloys with chemical compositions of Al-0.48Mg-1.03Si (wt.%) (Zn-free) and Al-0.48Mg-0.99Si-2.98 Zn (wt.%) (Zn-containing) were used in the present work. The as-cast alloys were homogenized at 500 °C for 10 h, and hot- and cold-rolled to 1 mm thick sheets. After that, these sheets were solution heat treated at 565 °C for 0.5 h and then quenched in cold water to room temperature. Finally, they were aged at 180 °C for different times in an oil bath.

Vickers hardness was measured with a load of 4.9 N and a dwell time of 10 s. The hardness values were the average values of at least 5 indentations. Transmission electron microscopy (TEM) and high-resolution TEM (HRTEM) observations were carried out with a FEI Tecnai F20 TEM operated at 200 KV. HAADF-STEM imaging was performed using an aberration-corrected FEI Titan Cubed Themis G2 operated at 300 kV. All microstructure images were taken along a $<100>_{Al}$ zone axis. The TEM/STEM specimens were prepared by electro-polishing using a Tenupol 5 machine (Struers) with an electrolyte of 1/3 HNO_3 in methanol at a temperature between -25 °C and−35 °C. In order to reduce the effect of contamination, all specimens were cleaned before HAADF-STEM observation using a Model 950 plasma cleaner (Gatan).

The first-principles calculations were performed using density functional theory (DFT) [30,31], which was implemented in the Vienna Ab initio Simulation Package (VASP) [32,33] with projector-augmented wave (PAW) potential [34,35]. The generalized gradient approximation (GGA) with the exchange-correlation function of Perdewe-Burkee-Ernzerhof (PBE) [36] was employed. Convergence tests indicated that 350 eV was sufficient cut-off energy for the PAW potential to achieve high precision in the current system. K-points sampling was carefully selected to ensure convergence in the order of a few meV $atom^{-1}$. The formation enthalpy of precipitate structures was calculated according to Ref. [37], which is proportional by inversion to the stability of the structures. The formation enthalpy of an $Al_xMg_ySi_zZn_m$ phase with respect to the solid solution is defined as:

$$\Delta H_{ss}\left(Al_xMg_ySi_zZn_m\right) = H\left(Al_xMg_ySi_zZn_m\right) - xH\left(Al^{fcc}\right) - yH\left(Mg^{sub}\right) - zH\left(Si^{sub}\right) - mH\left(Zn^{sub}\right) \quad (1)$$

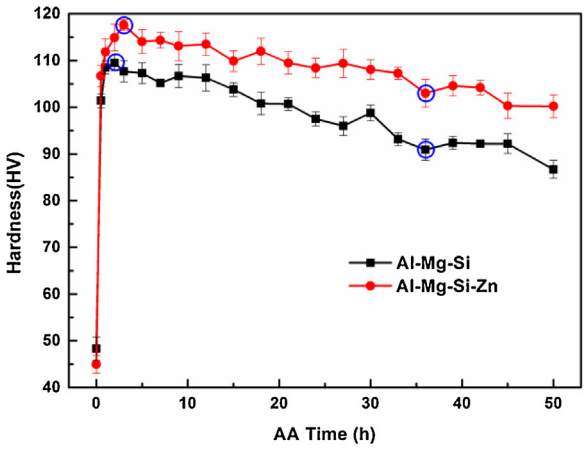

Fig. 1. Age-hardening curves of the two investigated alloys aged at 180 °C for different time.

where x, y, z and m are the atomic fractions ($x + y + z + m = 1$). The $H(Al_xMg_ySi_zZn_m)$ is the total energy of $Al_xMg_ySi_zZn_m$ phase per atom. $H(Mg^{sub})$, $H(Si^{sub})$ and $H(Zn^{sub})$ are the enthalpies of Mg, Si and Zn atoms on substitutional sites in the Al-matrix, respectively. The enthalpy $H(Mg^{sub})$ is calculated by employing 3 × 3 × 3 fcc Al supercells consisting of 108 atoms with a k-mesh of 11 × 11 × 11.

$$H\left(Mg^{sub}\right) = H\left(Al_{107}Mg\right) - \frac{107}{108}H\left(Al_{108}\right) \quad (2)$$

An analogous formula is valid for $H(Si^{sub})$ and $H(Zn^{sub})$.

It is worth mentioning that although the zero-vibration energy also contributes to the formation enthalpy of the precipitate phase, its contribution is small compared with other contributions, as has been demonstrated in previous work [38], and is therefore negligible in the calculations.

3. Results and discussion

3.1. Hardness measurements

Fig. 1 shows the age-hardening curves of the Zn-free and Zn-containing alloys aged at 180 °C. The hardness evolutions of these two alloys are similar, i.e., the hardness increases rapidly to a maximum value and then decreases gradually with increasing aging time. Compared with the Zn-free alloy, the Zn-containing alloy displays an overall higher hardness during the whole aging process. Apparently, Zn addition can enhance the age-hardening response of Al-Mg-Si alloys.

3.2. TEM and HRTEM observations

Four samples marked with blue circles in Fig. 1 were selected for TEM and HRTEM observations. Fig. 2(a) and (b) show the overall precipitate microstructures in the Zn-free and Zn-containing alloys at the peak-aged stage, respectively. In the Zn-free alloy, needle-like precipitates are uniformly dispersed in the Al-matrix with an average length of about 18 nm (Fig. 2(a)). In the Zn-containing alloy, it is interesting to see that apart from needle-like precipitates, there exists a small portion of lath-like precipitates in the matrix (as indicated by white arrows in Fig. 2(b)). The average length of the needle-like precipitates is about 9 nm, which is much smaller than that of the precipitates formed in the Zn-free alloy. With the aging time extending to 36 h (over-aged), the precipitates in both alloys become much coarser. Comparing the Zn-containing alloy with the Zn-free alloy, the needle-like precipitates formed in the

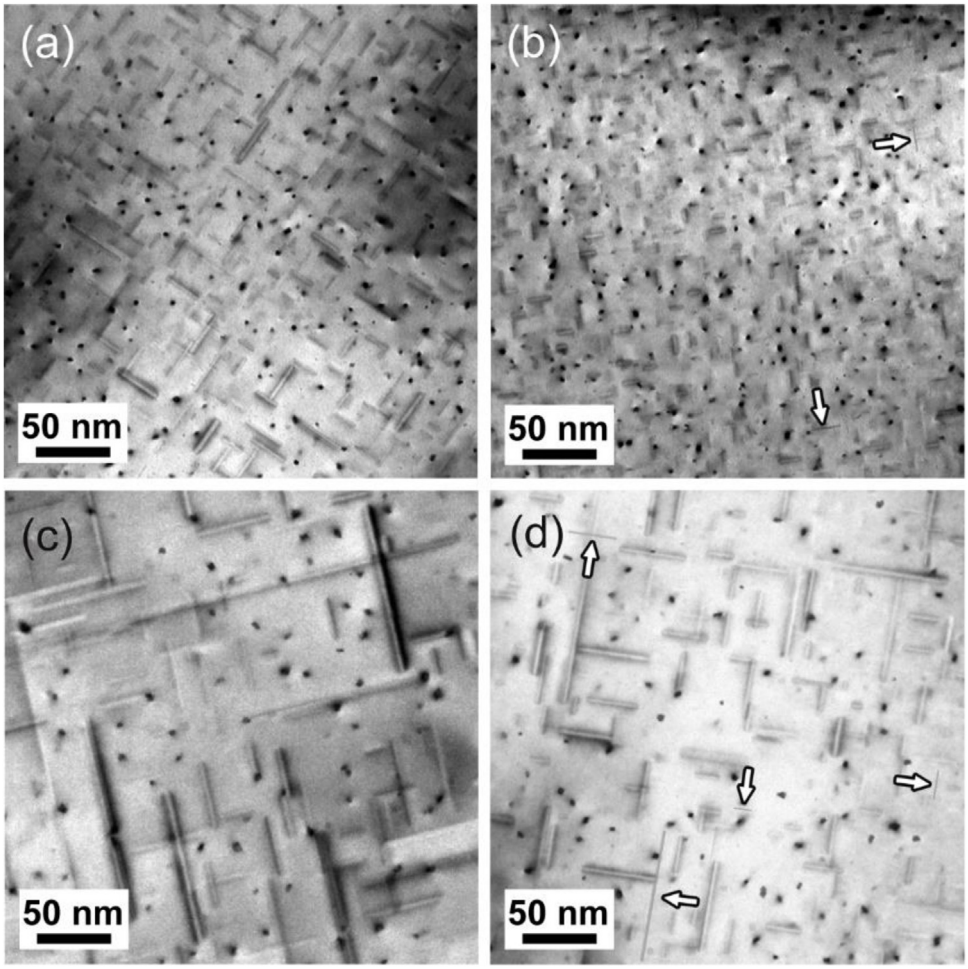

Fig. 2. TEM bright-field images of the two alloys peak-aged (a, b) and over-aged (c, d) at 180 °C. (a, c) Zn-free alloy, (b, d) Zn-containing alloy.

former alloy have the average length of 25 nm (Fig. 2(d)), which are much finer than those formed in the latter alloy (with an average length of 45 nm) (Fig. 2(c)). The lath-like precipitates can be observed in the Zn-containing alloy, as marked by white arrows in Fig. 2(d).

Conventional HRTEM observation shows that most of the precipitates formed in the Zn-free alloy under peak-aging and over-aging conditions are the β″-precipitates [8], as proved by the HRTEM images and corresponding fast Fourier-transform (FFT) patterns shown in Fig. 3. The lath-like precipitates formed in the Zn-containing alloy were found to have the same lattice structure as the Q'-phase [20], whose atomic structure can be deduced from the results shown in the next section. For the needle-like precipitates in the Zn-containing alloy, most of them have disordered structures in normal HRTEM imaging and are hardly to be identified. The detailed atomic structures of these precipitates will be revealed in the next section.

It has previously been demonstrated [22,26] that Zn addition to Al-Mg-Si alloys can result in a finer and denser distribution of needle-like precipitates. In the Zn-containing alloy studied in the present work, Zn element is observed to not only influence microstructure of the needle-like precipitates, but also induce the formation of the lath-like Q'-type precipitates. The above observed microstructure change should be responsible for the enhanced age-hardening response in the Zn-added alloy (Fig. 1).

3.3. HAADF-STEM characterization for Zn-containing alloy

Atomic-resolution HAADF-STEM examinations on hundreds of the precipitates in the Zn-containing alloy under peak-aged and over-aged conditions revealed that the needle-like precipitates have quite complicated structures. Representative needle-like precipitates for the peak-aged and over-aged conditions are presented in Figs. 5 and 6, respectively. For the sake of convenience in analyzing the images, Fig. 4 gives a schematic drawing of the unit cells of encountered known phases. Note that the structure portion(s) enclosed by circles, hexagons, triangles and triangle-like hexagon represent the characteristic sub-unit(s) of β″, U2, Q', and β'-2, respectively. The sub-unit of β″was referred to as "low density cylinder" (LDC) in previous Ref. [37]. Owing to the high resolution of the Z-contrast images, all atomic columns can be resolved in the structures. Zn columns appear as the much brighter dots because Zn has a much higher atomic number (Z = 30) than the other three elements (Z = 14 for Si, 13 for Al, and 12 for Mg) [39]. The structure models for all the HAADF-STEM images were based on the Z-contrast information, inter-atomic distances and local similarities with known phase structures in the Al-Mg-Si(-Cu) alloy system. It should be noted that all the atomic columns identified as Zn-containing ones are represented as Zn columns in the structure models, and in this paper no attempt is made to clarify the levels of Zn occupancy in those columns. For the peak-aged condition (Fig. 5), composite precipitates are dominant and only

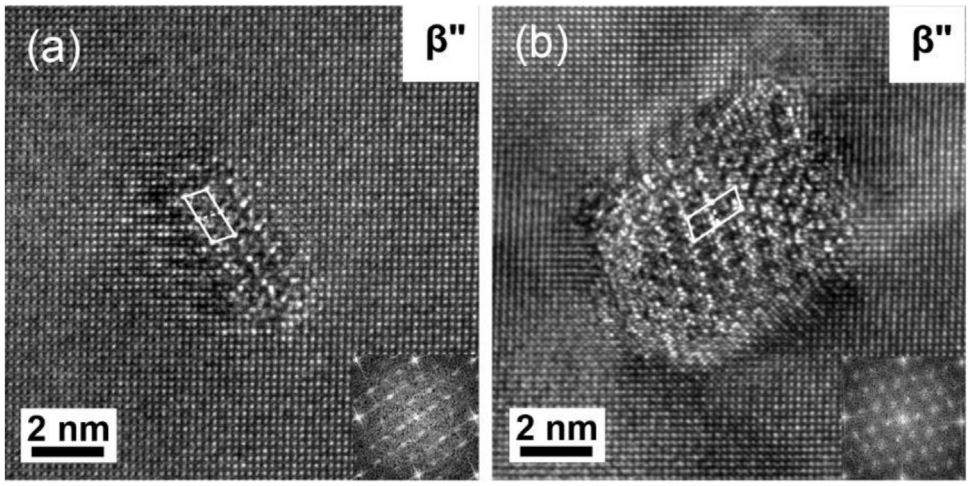

Fig. 3. HRTEM images of the typical precipitates formed in the Zn-free alloy after peak-aging (a) and over-aging (b) at 180 °C. The inset in each image is the corresponding FFT pattern.

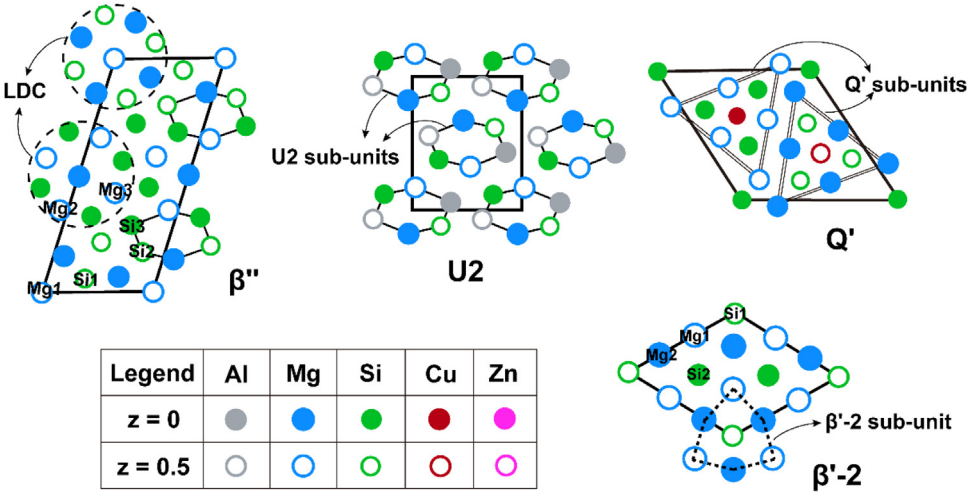

Fig. 4. Legend representing the structure models in Figs. 5 and 6 and schematic drawing of the unit cell of β″, U2, Q' and β'-2. The characteristic sub-unit(s) of the four phases are marked by dashed-line circles, solid-line hexagons, double-solid-line triangles and dashed-line triangle-like hexagon, respectively.

a small portion of pure β″-precipitates (a typical one is shown in Fig. 5(a)) is observed among the needle-like precipitates. A similar phenomenon was reported in a previous study [22]. After 36 h aging (Fig. 6), it is seen that almost all of the needle-like precipitates become composite precipitates. It is worth mentioning that the fraction of each phase in the composite precipitates for both aging conditions varies from one precipitate to another. In addition, the overall structural feature of the composite precipitates in the over-aged condition is similar to that in the peak-aged condition, though the cross-sections of the former show a modest coarsening relative to those of the latter. The following observations can be made from Figs. 5 and 6.

- The contrast of Al columns in the vicinity of the precipitate interfaces with the matrix tends to be stronger than that of the normal Al columns. This strongly indicates that Zn atoms segregate at the precipitate/matrix interfaces by replacing Al atoms in the matrix, which is consistent with previous work [[22]].
- For the composite precipitate shown in Fig. 5(c), sub-units of β″(LDC), U2, β' and Q' coexist within the precipitate, lacking long-range periodicity of the four phases. In the upper left part of the precipitate, one unit cell of the Q'-phase is observed. A striking feature is that all of the phases involved have some atomic columns replaced (partly or totally) by Zn. We refer to the four Zn-containing phases as β″Zn, U2Zn, β'Zn and Q'Zn, respectively.
- The precipitate shown in Fig. 6(a) consists of three structures. In the left part of the precipitate, unit cells of β″Zn can be identified. Unit cells of U2Zn connect to the unit
- cells of β″Zn. In the right part of the precipitate, sub-units of β'Zn are observed. For the precipitate shown in Fig. 6(c), unit cells and sub-units of U2Zn, β'Zn and Q'Zn are clearly seen.
- The β″Zn phase is formed by Zn atoms replacing the Si3 atoms in the β″unit cell, which has the same structure as the β″Zn phase reported in Ref. [[27]]. For the U2Zn phase, Zn atoms are assumed to be incorporated at the Al sites in the U2 unit cell. In fact, these sites are locally identical to the Si3 sites in the β″-phase, as the β″and U2 phases show close structural similarities (see Fig. 4). The Q'Zn phase has the same structure as the Q'-phase formed in Al-Mg-Si-Cu alloys [[20]], except for the Cu atoms are replaced by Zn atoms. Note that the unit cell of the lath-like Q'-precipitates formed in the Zn-containing alloy is isostructural with the Q'Zn unit cell.
- The β'Zn phase is formed by Zn atoms replacing the Si1 and Mg2 atoms in the β'-2 unit cell. Moreover, the Si1 and Mg2 columns have comparable intensities with the brightest Zn columns at the precipitate/matrix interfaces. If these brightest Zn columns are

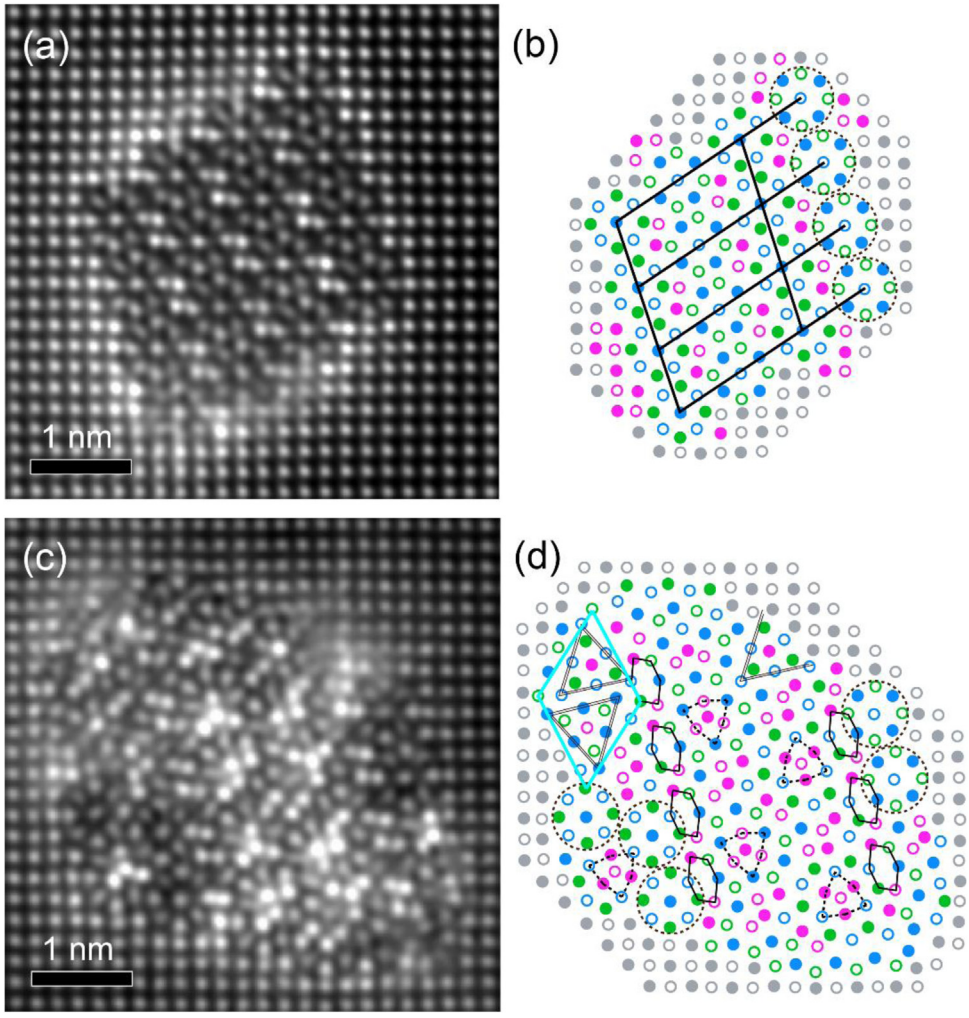

Fig. 5. Atomic-resolution HAADF-STEM images of β"$_{Zn}$-precipitate (a) and β"$_{Zn}$/U2$_{Zn}$/β'$_{Zn}$/Q'$_{Zn}$ composite precipitate (c) formed in the Zn-containing alloy peak-aged at 180 °C. (b) and (d) are suggested structure models for the images (a) and (c), respectively. See legend in Fig. 4.

assumed to contain Zn with full occupancy (based on the assumption that Zn, having a similar atomic radius with Al, can easily replace Al), it gives a sufficient reason to consider full Zn occupancy at the Si1 and Mg2 sites. This generates a β'$_{Zn}$ composition as $Mg_3Si_2Zn_4$.

The above observations have clearly shown that Zn atoms can enter all the hardening phases involved to occupy specific featured atomic sites of the original elements and modify their crystal structures, interfacial structures and morphologies in characteristic manners. Another interesting phenomenon is that the single-phase β'$_{Zn}$-precipitates and the single-phase U2$_{Zn}$-precipitates do not exist in the Al-Mg-Si-Zn alloy. Instead, they either coexist with β"$_{Zn}$ or with Q'$_{Zn}$ to form multiphase composite precipitates. Comparing the role of Zn with that of other additive alloying elements such as Ag and Cu in the precipitate structures in the Al-Mg-Si(-Cu) alloy system, it is interesting to note that for the β", U2 and Q' phases, Zn atoms occupy similar atomic sites as Ag and Cu do [20,27,29,40], whereas for the β'-phase, they occupy unique atomic sites.

The HAADF-STEM results in association with the TEM results have demonstrated that the precipitates formed in the Zn-free alloy are the most effective hardening β"-precipitates, while the precipitates formed in the Zn-containing alloy mainly are the relatively finer composite precipitates. A better age-hardening response is observed for the latter alloy relative to the former alloy, suggesting that the composite precipitates are capable of effectively hardening the alloys, though the late-stage phase structures (i.e., β'$_{Zn}$ and U2$_{Zn}$) are frequently present in these precipitates.

3.4. First-principles study of stability of β'-type phases

In this section, we utilize first-principles calculations to understand the effect of Zn on the β'-phase and the difference between the effect of Zn and that of Ag on this phase. The formation enthalpies (ΔH) of Zn-containing β'-2 phase structures with different atomic sites replaced by Zn were calculated and the results are shown in Fig. 7. The ΔH of Zn-free β'-2 phase is also given for comparison. It can be seen that the three unit cells formed by Zn replacing each of the Si1, Si2 and Mg2 sites have lower ΔH while the one formed by Zn replacing the Mg1 site has significantly higher ΔH than the β'-2 unit cell. This indicates that the Si1, Si2 and Mg2 sites are the energetically-preferred sites for Zn substitution in the β'-2 unit cell. We further calculated the ΔH of unit cells formed by Zn replacing two of the energetically-preferred sites. The results demonstrate that the unit cell formed by Zn replacing the Si1 and Mg2 sites (i.e., the β'$_{Zn}$ phase observed in this paper) has the lowest ΔH among all the considered Zn-containing structures (Fig. 7), implying that the formation of this structure is energetically favorable, which corresponds well to the experimental results (Figs. 5(c)and 6).

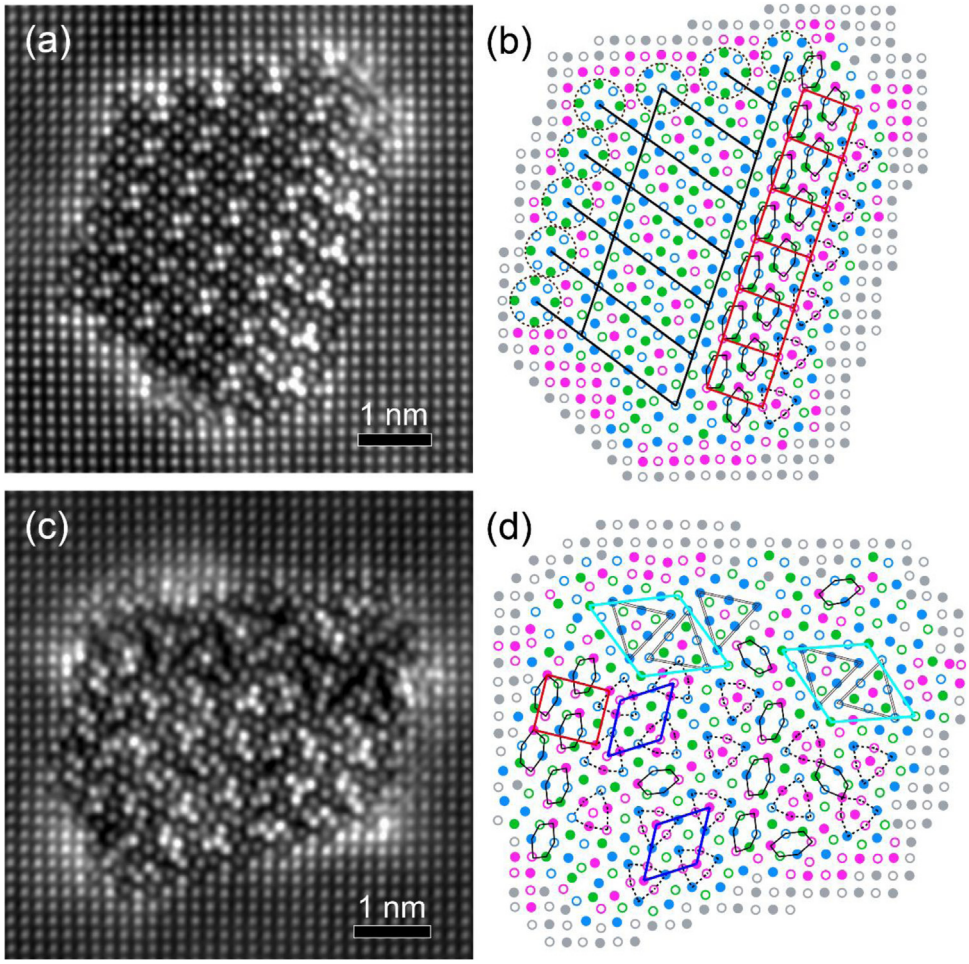

Fig. 6. Atomic-resolution HAADF-STEM images of β"$_{Zn}$/U2$_{Zn}$/β'$_{Zn}$ (a) and U2$_{Zn}$/β'$_{Zn}$/Q'$_{Zn}$ (c) composite precipitates formed in the Zn-containing alloy over-aged at 180 °C for 36 h. (b) and (d) are suggested structure models for the images (a) and (c), respectively. See legend in Fig. 4.

Table 1
Comparison between the crystal structure of β'$_{Zn}$ and β'$_{Ag}$ unit cells.

	β'$_{Zn}$					β'$_{Ag}$ [28]				
Lattice parameters	$a = b$ =0.690 nm, c =0.405 nm					$a = b$ =0.690 nm, c =0.405 nm				
Space group	P-62 m (hexagonal)					P-62 m (hexagonal)				
Composition	$Mg_3Si_2Zn_4$					$Mg_3Al_3Si_2Ag$				
Atomic position	Atom	x	y	z	Occ.	Atom	x	y	z	Occ.
	Zn1	0	0	0	1	Ag	0	0	0	1
	Si	1/3	2/3	1/2	1	Si	1/3	2/3	1/2	1
	Mg	0.4	0.4	0	1	Mg	0.4	0.4	0	1
	Zn2	0.74	0.74	1/2	1	Al	0.74	0.74	1/2	1

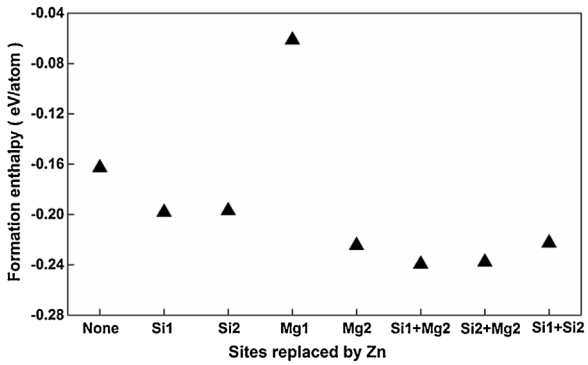

Fig. 7. The formation enthalpies of β'-2 unit cells with different atomic sites replaced by Zn.

Comparing the structure of the β'$_{Zn}$ phase with that of the β'$_{Ag}$ phase reported in Ref. [28] (see Fig. 8 and Table 1), it is apparent that Zn and Ag additions in Al-Mg-Si alloys change the β'-2 phase structure in different manners. The additions of these two elements only lead to modification of the atom types at the Si1 and Mg2 sites in the β'-2 phase. In the case of Zn addition, both the Si1 and Mg2 sites are replaced by Zn. While in the case of Ag addition, the Si1 site is replaced by Ag, but the Mg2 site by Al rather than by Ag. One question arises from the above observations: why does Ag only replace the Si1 site, whereas Zn replaces both the Si1 and Mg2 sites? To answer the question, we again did first-principles calculations. Two structure models according to the β'$_{Zn}$ and β'$_{Ag}$ structures were considered: One is $Mg_3Si_2X_4$ cell built by atom X (Zn or Ag) replacing the Si1 and Mg2 sites in the β'-2 phase. The second one is $Mg_3Al_3Si_2X$ cell obtained by atom X replacing the Si1 site and Al replacing the Mg2 site. The ΔH of the four possi-

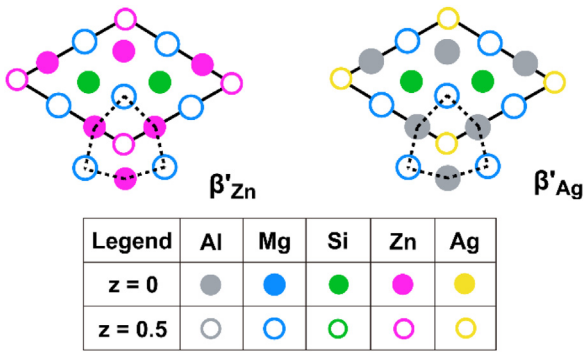

Fig. 8. Schematic drawing of the atomic structures of β'_{Zn} and β'_{Ag} phases.

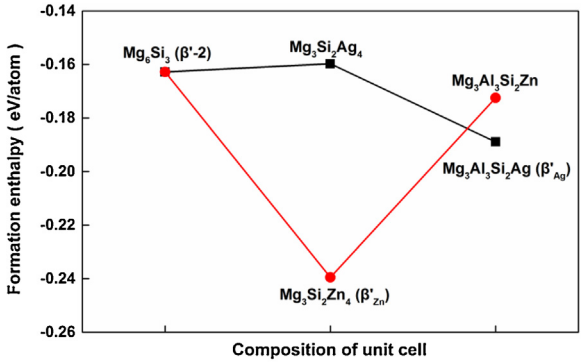

Fig. 9. Formation enthalpies of modified β'-2 unit cells plotted as a function of composition.

ble unit cells is shown in Fig. 9. From the black line in Fig. 9, it is clear that $Mg_3Al_3Si_2Ag$ has lower ΔH than $Mg_3Si_2Ag_4$, indicating that the formation of the former structure is energetically favorable. This is consistent with the experimental result [28]. Nevertheless, the opposite trend appears for the Zn-containing structures that $Mg_3Si_2Zn_4$ has much lower ΔH than $Mg_3Al_3Si_2Zn$ (see the red line in Fig. 9). Again, the first-principles calculation result matches well with the experimental result that Zn replaces both the Si1 and Mg2 sites in β'-2. Further investigation of the electronic structure and bonding nature [41] of the β'_{Zn} and β'_{Ag} phases may provide useful information to understand the underlying mechanism for the different modifications of the β'-2 structure caused by different additive alloying elements.

4. Conclusions

We have employed atomic-resolution HAADF-STEM and first-principles calculations to investigate the atomic-scale roles of Zn addition in alloying an age-hardened Al-Mg-Si-Zn alloy. From the obtained results, the following can be concluded.

(1) Significant amount of Zn atoms can be added into the Al-Mg-Si alloy and they can easily enter the bulk structures of many known hardening phases at energetically favorable atomic sites, forming Zn-containing β''_{Zn}, β'_{Zn}, $U2_{Zn}$ and Q'_{Zn} phase structures. In addition, Zn atoms will modify the precipitate morphologies and the interfaces between precipitates, and between the precipitates and the Al-matrix.

(2) The single-phase β'_{Zn}-precipitates and the single-phase $U2_{Zn}$-precipitates cannot be observed to exist. Upon formation, they either coexist as the composite precipitates associated with β''_{Zn}, or associated with Q'_{Zn}.

(3) For the β'-phase, Zn atoms occupy unique atomic sites, whereas for other phases, they occupy similar atomic sites as other additive alloying elements such as Ag and Cu do. In the modified β'_{Zn}-phase structure, Zn atoms will replace both Si-atoms and Mg-atoms at specific sites of the original β'-2 structure, changing the composition from Mg_6Si_3 to $Mg_3Si_2Zn_4$.

Acknowledgements

This work was financially supported by the National Key Research and Development Program of China (No. 2016YFB0300801) and the National Natural Science Foundation of China (Nos. 51831004, 11427806, 51671082, 51471067). We acknowledge Electron Microscopy Laboratory at Peking University for the use of aberration-corrected electron microscope.

References

[1] S. Pogatscher, H. Antrekowitsch, H. Leitner, T. Ebner, P.J. Uggowitzer, Acta Mater. 59 (2011) 3352–3363.
[2] W.S. Miller, L. Zhuang, J. Bottema, A.J. Wittebrood, P.D. Smet, A. Haszler, A. Vieregge, Mater. Sci. Eng. A 280 (2000) 37–49.
[3] J.M. Hu, W.G. Zhang, D.F. Fu, J. Teng, H. Zhang, J. Mater. Res. Technol. 8 (2019) 5950–5960.
[4] J.M. Hu, J. Teng, X.K. Ji, D.F. Fu, W.G. Zhang, H. Zhang, Mater. Sci. Eng. A 695 (2017) 35–44.
[5] X.K. Ji, H. Zhang, S. Luo, F.L. Jiang, D.F. Fu, Mater. Sci. Eng. A 649 (2016) 128–134.
[6] G.A. Edwards, K. Stiller, G.L. Dunlop, M.J. Couper, Acta Mater. 46 (1998) 3893–3904.
[7] J.H. Chen, E. Costan, M.A. van Huis, H.W. Zandbergen, Science 312 (2006) 416–419.
[8] H.W. Zandbergen, Science 277 (1997) 1221–1225.
[9] S.J. Andersen, H.W. Zandbergen, J. Jansen, C. Traeholt, U. Tundal, O. Reiso, Acta Mater. 46 (1998) 3283–3298.
[10] P.H. Ninive, A. Strandlie, S. Gulbrandsen-Dahl, W. Lefebvre, C.D. Marioara, S.J. Andersen, J. Friis, R. Holmestad, O.M. Løvvik, Acta Mater. 69 (2014) 126–134.
[11] R. Vissers, M.A. van Huis, J. Jansen, H.W. Zandbergen, C.D. Marioara, S.J. Andersen, Acta Mater. 55 (2007) 3815–3823.
[12] K. Matsuda, Y. Sakaguchi, Y. Miyata, J. Mater. Sci. 35 (2000) 179–189.
[13] A.G. Frøseth, R. Høier, P.M. Derlet, S.J. Andersen, C.D. Marioara,Phys. Rev. B 67 (2003), 224106.
[14] S.J. Andersen, C.D. Marioara, A. Frøseth, R. Vissers, Mater. Sci. Eng. A 444 (2007) 157–169.
[15] S.J. Andersen, C.D. Marioara, A. Frøseth, R. Vissers, H.W. Zandbergen, Mater. Sci. Eng. A 390 (2005) 127–138.
[16] J.K. Sunde, C.D. Marioara, A.T.J. van Helvoort, R. Holmestad, Mater. Charact. 142 (2018) 458–469.
[17] Y.X. Lai, B.C. Jiang, C.H. Liu, Z.K. Chen, C.L. Wu, J.H. Chen, J. Alloys. Compd. 701 (2017) 94–98.
[18] Y.X. Lai, W. Fan, M.J. Yin, C.L. Wu, J.H. Chen, J. Mater. Sci. Technol. 41 (2020) 127–138.
[19] C.H. Liu, Y.X. Lai, J.H. Chen, G.H. Tao, L.M. Liu, P.P. Ma, C.L. Wu, Scr. Mater. 115 (2016) 150–154.
[20] C. Wolverton, Acta Mater. 49 (2001) 3129–3142.
[21] M.X. Guo, G. Sha, L.Y. Cao, W.Q. Liu, J.S. Zhang, L.Z. Zhuang, Mater. Chem. Phys. 162 (2015) 15–19.
[22] T. Saito, S. Wenner, E. Osmumdsen, C.D. Marioara, S.J. Andersen, J. Røyset, W. Lefebvre, R. Holmestad, Philos. Mag. Abingdon (Abingdon) 94 (2014) 2410–2425.
[23] X.P. Ding, H. Cui, J.X. Zhang, H.X. Li, M.X. Guo, Z. Lin, L.Z. Zhuang, J.S. Zhang, Mater. Des. 65 (2015) 1229–1235.
[24] L. Yan, Y. Zhang, X. Li, Z. Li, F. Wang, H. Liu, B. Xiong, Prog. Nat. Sci. Mater. Int. 24 (2014) 97–100.
[25] M.X. Guo, X.K. Zhang, J.S. Zhang, L.Z. Zhuang, J. Mater. Sci. 52 (2017) 1390–1404.
[26] S. Zhu, Z.H. Li, L.Z. Yan, X.W. Li, S.H. Huang, H.W. Yan, Y.A. Zhang, B.Q. Xiong, Mater. Charact. 145 (2018) 258–267.
[27] T. Saito, F.J.H. Ehlers, W. Lefebvre, D. Hernandez-Maldonado, R. BjØrge, C.D. Marioara, S.J. Andersen, R. Holmestad, Acta Mater. 78 (2014) 245–253.
[28] C.D. Marioara, J. Nakamura, K. Matsuda, S.J. Andersen, R. Holmestad, T. Sato, T. Kawabata, S. Ikeno, Philos. Mag. Abingdon (Abingdon) 92 (2012) 1149–1158.
[29] Y.Y. Weng, L.P. Ding, Z.Z. Zhang, Z.H. Jia, B.Y. Wen, Y.Y. Liu, S. Muraishi, Y.J. Li, Q. Liu, Acta Mater. 180 (2019) 301–316.
[30] P. Hohenberg, W. Kohn, Phys. Rev. B 136 (1964) 864–871.
[31] W. Kohn, L.J. Sham, Phys. Rev. A (Coll Park) 140 (1965) 1133–1138.
[32] G. Kresse, J. Hafner, Phys. Rev. B 47 (1993) 558–561.
[33] G. Kresse, J. Furthmller, Phys. Rev. B 54 (1996) 11169–11186.
[34] G. Kresse, D. Joubert, Phys. Rev. B 59 (1999) 1758–1775.
[35] P.E. Blochl, Phys. Rev. B 50 (1994) 17953–17979.

[36] J.P. Perdew, K. Burke, M. Ernzerhof, Phys. Rev. Lett. 77 (1996) 3865–3868.
[37] M.A. van Huis, J.H. Chen, H.W. Zandbergen, M.H.F. Sluiter, Acta Mater. 54 (2006) 2945–2955.
[38] Z.R. Liu, J.H. Chen, S.B. Wang, D.W. Yuan, M.J. Yin, C.L. Wu, Acta Mater. 59 (2011) 7396–7405.
[39] T. Yamazaki, M. Kawasaki, K. Watanabe, I. Hashimoto, M. Shiojiri, Ultramicroscopy 92 (2002) 181–189.
[40] K. Li, A. Beche, M. Song, G. Sha, X.X. Lu, K. Zhang, Y. Du, S.P. Ringer, D. Schryvers, Scr. Mater. 75 (2014) 86–89.
[41] L.P. Ding, Z.H. Jia, J.F. Nie, Y.Y. Weng, L.F. Cao, H.W. Chen, X.Z. Wu, Q. Liu, Acta Mater. 145 (2018) 437–450.